NASA TECHNICAL NOTE

NASA TN D-7999

NASA TN D-7999

CROSSFLOW IN TWO-DIMENSIONAL ASYMMETRIC NOZZLES

Daniel I. Sebacher and Louise P. Lee

Langley Research Center
Hampton, Va. 23665

NATIONAL AERONAUTICS AND SPACE ADMINISTRATION • WASHINGTON, D. C. • AUGUST 1975

1. Report No.	2. Government Accession No.	3. Recipient's Catalog No.
NASA TN D-7999		

4. Title and Subtitle	5. Report Date
CROSSFLOW IN TWO-DIMENSIONAL ASYMMETRIC NOZZLES	August 1975
	6. Performing Organization Code

7. Author(s)	8. Performing Organization Report No.
Daniel I. Sebacher and Louise P. Lee	L-10072
	10. Work Unit No.
9. Performing Organization Name and Address	505-05-41-03
NASA Langley Research Center Hampton, Va. 23665	11. Contract or Grant No.
	13. Type of Report and Period Covered
12. Sponsoring Agency Name and Address	Technical Note
National Aeronautics and Space Administration Washington, D.C. 20546	14. Sponsoring Agency Code

15. Supplementary Notes

16. Abstract

An experimental investigation of the crossflow effects in three contoured, two-dimensional asymmetric nozzles is described. The data are compared with theoretical predictions of nozzle flow by using an inviscid method of characteristics solution and two-dimensional turbulent boundary-layer calculations. The effect of crossflow as a function of the nozzle maximum expansion angle is studied by use of oil-flow techniques, static wall-pressure measurements, and impact-pressure surveys at the nozzle exit. Reynolds number effects on crossflow are investigated.

17. Key Words (Suggested by Author(s))	18. Distribution Statement
Crossflow 2-D nozzle	Unclassified – Unlimited Subject Category 34

19. Security Classif. (of this report)	20. Security Classif. (of this page)	21. No. of Pages	22. Price*
Unclassified	Unclassified	31	$3.75

*For sale by the National Technical Information Service, Springfield, Virginia 22161

CROSSFLOW IN TWO-DIMENSIONAL ASYMMETRIC NOZZLES

Daniel I. Sebacher and Louise P. Lee
Langley Research Center

SUMMARY

An experimental investigation of the crossflow effects in three contoured, two-dimensional asymmetric nozzles is described and results are compared with theoretical predictions of nozzle flow by use of an inviscid method of characteristics solution and two-dimensional turbulent boundary-layer calculations. The nozzles varied in maximum expansion angle from 15°17' to 29°20' but all were designed for the same area ratio to give an exit Mach number of 3.49 by use of expanding air at a stagnation temperature of 290 K. The results of this study show that crossflow takes place in the boundary layer of all the test nozzles. Exit pitot-pressure surveys and sideplate oil drop flows illustrate the trade-off between increased crossflow driving force in the larger turning angle nozzle to the thicker boundary-layer buildup in the longer, smaller turning angle nozzle. Static wall-pressure measurements were found to agree well with the inviscid method of characteristics theory when it is assumed that no crossflow and a relatively undisturbed flow core suitable for wind-tunnel testing exists for the three nozzles.

INTRODUCTION

Test facilities (ref. 1) tailored to investigate rectangular scramjet engine configurations for the integrated scramjet engine-airframe concept (ref. 2) will probably utilize a rectangular nozzle exit which is generally obtained by some type of two-dimensional expansion. Two-dimensional asymmetric nozzle configurations consisting of a contoured wall, a flat bottom plate, and flat sidewalls have been considered for use in both the integrated scramjet engine-airframe concept and the wind-tunnel test facility and are the subject of this report. One problem associated with this type of nozzle is the development of lateral pressure gradients on the nozzle sidewalls induced by streamline curvature which can result in boundary-layer crossflow along the sidewalls in a direction normal to the potential flow streamlines. These lateral pressure gradient effects will appear as lower pressure along the contoured wall compared with the pressure at the same station along the bottom plate in the region of the initial circular-arc expansion and as higher pressures along the contoured wall when the flow is turned back parallel downstream of the maximum turning angle. The nozzles designed for this study will also contain a region

of parallel flow where design pressure has been achieved first along the bottom plate and then through the flow core to the nozzle exit on the contoured wall. In this region of uniform pressure, the previous driving force for crossflow vanishes, but the difference in streamline direction between the flow core and the boundary layer will further modify the boundary-layer flow by viscous interaction.

Since the use of the two-dimensional asymmetric nozzles has been limited and generally confined to small expansion angles, the effects of crossflow in these nozzles have largely been ignored. A related investigation of secondary flows in the convergent region of planar nozzles is reported in reference 3, and an analysis of crossflow in laminar flow with boundary-layer control using suction is given in reference 4. A novel study of the use of fences to decrease crossflow effects on a nozzle sidewall is found in reference 5.

To determine the effects of crossflow as a function of maximum nozzle turning angle, the flow characteristics of three contoured two-dimensional asymmetric nozzles are investigated experimentally and the results are compared with nozzle flow predictions by using an inviscid method of characteristics solution and two-dimensional boundary-layer theory. Any significant distortion of the flow core due to crossflow is of particular interest because of the possible application of nozzles of this type to integrated engine-airframe, hypersonic aircraft configurations. (See ref. 2.)

SYMBOLS

h^*	throat height (see fig. 1(b))
N_{Re}	Reynolds number (based on flow speed at nozzle throat and throat height)
p_{bp}	static pressure on nozzle bottom plate
p_{cw}	static pressure on nozzle contoured wall
p_t	stagnation chamber pressure
$p_{t,2}$	impact pressure
p_w	static pressure on sidewalls
x,y,z	nozzle coordinates (see fig. 1(a))
θ_{max}	nozzle maximum expansion angle

Abbreviations:

2-D two-dimensional

MOC method of characteristics

APPARATUS AND METHOD

Nozzles

A preliminary design analysis, using the method of characteristics solution, indicated that for the flow conditions available for this experiment, a suitable range of the sidewall pressure gradients causing crossflow in two-dimensional asymmetric nozzles could be achieved with θ_{max} between 15° and 29°. Therefore, three contoured nozzles with nominal values of θ_{max} of $15^{\circ}17'$, $23^{\circ}23'$, and $29^{\circ}20'$ were selected for investigation as shown in figure 1. The three nozzles were identical upstream of the throats and all were designed to expand 290 K air to a free-stream Mach number of 3.49. The length of each nozzle wall was terminated at the location that theoretical calculations indicated parallel flow would be achieved; this termination resulted in a decreasing nozzle length as the maximum expansion angle was increased. The length of the nozzles were 42.10 cm, 31.10 cm, and 26.62 cm for nozzles with maximum expansion angles of $15^{\circ}17'$, $23^{\circ}23'$, and $29^{\circ}20'$, respectively. For the three nozzles, the width was 7.62 cm, the throat height was 0.847 cm, and the exit height was 6.10 cm. The stagnation chamber housed a permanent flow straightener, as shown in figure 1(b). The nozzle sidewalls were sealed at the contact surfaces of the contoured top plate and the flat bottom plate.

Instrumentation

The strain-gage pressure transducers used in this experiment have a rated measurement accuracy of ±0.5 percent. The output from the transducers is recorded on tape and converted to a digitized readout by using a calibration tape; therefore, the usual errors involved in reading a visual recording are not applicable. On the other hand, there are errors involved in the recording readout system due to instrument drift and systematic calibration inaccuracies which have been estimated to be ±2 percent by comparing the system readout with a number of direct measurements. The random error of the recording system due to noise is given as ±0.2 percent by the manufacturer. The maximum error for the pressure ratios presented in this report is ±5.4 percent.

The impact pressure probe used to survey the boundary layer and flow core at the nozzle exit plane had a circular cross section with an outside diameter of 0.1 cm. The

probe was 5.23 cm long and was attached to a wedge-shaped strut of the same thickness which, in turn, was remotely controlled by a motor-driven screw which permitted travel in a direction normal to nozzle walls. The impact-pressure measurements were recorded on digital tape and sampled every 0.1 second and thus gave a data point every 0.044 cm in the y-direction. A traverse was taken every 0.5 cm in the z-direction from the sidewall to 0.5 cm past the center line of the nozzle.

The static wall pressure orifices have a diameter of 0.15 cm and are connected to the pressure transducers by a short piece of stainless-steel tubing of the same inside diameter. The coordinates of the static wall-pressure orifices are found in tables I and II. The wall static pressures and impact pressures were measured during the same runs and recorded on tape along with the stagnation chamber pressure, probe position, and airflow rate.

The oil-flow studies consisted of splattering small quantities of a mixture of lampblack and silicone oil over the area of the sideplates before each run, and observing the flow pattern of the mixture after a quick release valve initiated the airflow. A plexiglass sideplate was used on one side of the nozzle so that the oil flow could be observed during the run. Several seconds of flow time were required to obtain a useful flow pattern which could be photographed and once the flow pattern was set, no drift was observed when left to stand over a period of days if a proper mixture of lampblack and oil was initially applied. When a thin coat of silicone oil was rubbed into the sidewall prior to splattering the oil-flow mixture, the quality of the flow patterns was improved.

Test Conditions and Procedures

All three nozzles expanded 290 K dried air, with an H_2O mole fraction less than 2×10^{-4}, to a free-stream Mach number of 3.49. The nozzle flow was exhausted into an evacuated chamber maintained at 5 mm Hg. Stagnation pressure varied from 220 to 372 kN/m^2 and resulted in a Reynolds number range of 2.75×10^5 to 4.64×10^5 based on flow conditions at the nozzle throat and throat height. These conditions along with the physical size of the nozzles were largely limited by the maximum mass flow of dry air available which was 0.68 kg/sec.

METHOD OF CALCULATION

Nozzle Contouring

The numerical technique for determining the contours for the two-dimensional asymmetric nozzles used the method of characteristics for a rotational gas mixture. The stagnation enthalpy is allowed to vary normal to the streamlines. (See refs. 6 and 7.) Since only expanding 290 K air was considered, this analysis assumes each component of

the gas to be thermally perfect. Properties for the chemical species of air as a function of temperature, as needed for this method, are presented in reference 8. Initial uniform profiles of velocity, temperature, pressure, flow inclination, and mass fraction at the nozzle throat for starting the contouring program are also calculated by assuming a thermally perfect gas. (See ref. 9.)

When using the method of characteristics solution for computing the three nozzle contours shown in figure 1(b), the flow was initially expanded through a circular-arc contour of specified radius to a point of maximum turning angle from which the downrunning characteristic line yields the design pressure on the nozzle axis. For the flow conditions and exit Mach number of these nozzles, the maximum turning angle is a strong function of the initial circular arc up to a θ_{max} of about 29°, after which the maximum turning angle becomes insensitive to decreasing the initial circular arc.

The method of characteristics solution will also predict the inviscid static-pressure distribution on the nozzle walls and throughout the flow field. The results of these calculations were not only used as a comparison with the measured static pressures, but were also needed as input to the boundary-layer calculations. The analytical program used to compute the nozzle contours had a number of other computational options available but only those needed in this study have been described. Proper grid spacing was determined to insure accuracy in these solutions and the program's iteration procedure usually converged in three iterations. Coordinates for the three nozzles investigated are found in table III.

Boundary-Layer Calculations

Solutions of two-dimensional laminar and turbulent boundary-layer equations for multicomponent nonreacting gases were used in the boundary-layer analysis. The boundary-layer equations are transformed by the Levy-Lees transformation equations. These solutions (ref. 10) used an implicit finite-difference scheme for two-dimensional nozzles. The energy equation is written in terms of the stagnation enthalpy and the Reynolds' shear, and conductivity terms are given by an eddy viscosity and the turbulent Prandtl number.

The turbulent analysis employs the eddy viscosity law derived by Reichardt in the region of the boundary layer near the wall and follows Clauser's work using Klebanoff's intermittency factor in the outer part of the boundary layer. Reference 11 presents the system of equations describing the fluid flow in a boundary layer and a FORTRAN program used to solve these equations. This program has the capability of handling two-dimensional laminar or turbulent boundary-layer flows and the transition from laminar to turbulent flow. The computational step size along the wall is varied throughout the nozzle

depending on the pressure gradient at each point. The boundary-layer wall pressure distribution was determined by using the inviscid method of characteristics solution.

RESULTS AND DISCUSSION

Nozzle Differential Pressure

The nondimensional differential pressures between the contoured wall (p_{cw}) and the bottom plate (p_{bp}) of the asymmetric nozzles computed by the inviscid theory are shown in figure 2 as a function of axial distance. These pressure differentials for the three nozzles illustrate the crossflow driving force in terms of pressure gradient variations along the nozzle sidewalls. The initial dip in the pressure differential takes place because the flow first expands more rapidly along the circular-arc contour than along the bottom plate. Once the wall curvature reverses and begins to turn the flow back parallel to the nozzle bottom plate, the pressure on the contoured wall becomes greater than the pressure on the bottom plate. The reversal of the streamline curvature therefore causes the pressure differential to increase to zero, then go positive, and again decrease to zero as the nozzle exit is approached. Both the position of the pressure differential peak and its magnitude should affect the degree of crossflow in these nozzles. The maximum pressure differential not only takes place at a point of greater pressure in the higher turning angle nozzles but also farther upstream in the critical region just downstream of the throat. This maximum pressure differential decreases in magnitude and its locus moves downstream as the turning angle is decreased. The nozzles designed for this study also contain a region of parallel flow where design pressure has been achieved first along the bottom plate and through the flow core to the nozzle exit on the contoured wall as indicated by the area downstream of the parallel flow characteristic lines in figure 1(b). In this region of uniform pressure the previous driving force for crossflow vanishes.

Oil Flows

Experimental verification of the boundary-layer crossflow normal to the inviscid flow streamlines is shown in the oil-flow studies presented in figure 3. Any upward crossflow from the bottom plate toward the contoured wall due to the initial negative pressure gradient indicated in figure 2 is not readily discernible for any of the nozzles in figure 3. On the other hand, the downward crossflow from the contoured wall to the bottom plate is obvious in these photographs for all three nozzles because of the large broad positive gradients shown in figure 2. The streamlines start to become parallel to the bottom plate as the exit is approached. In this region of uniform pressure the crossflow driving force vanishes, but the difference in streamline direction between the flow core and the boundary layer will further modify the boundary-layer flow direction by viscous interaction. Additional crossflow effects have been observed in the test sections of the

two-dimensional nozzles with constant cross-section extensions (refs. 12 and 13) but the flow region past the nozzle exit is not considered in this study. A typical predicted streamline with no crossflow has been included in figure 3 to indicate the direction of the core flow.

Wall-Pressure Measurements

Wall-pressure measurements were taken along the center line of the contoured plate and the bottom plate, and also at various locations on a grid inscribed on the sideplate for each nozzle configuration. (See tables I and II.) These data are presented as the pressure difference between the contoured and bottom plates as a function of axial distance in figure 4 and as sidewall isobars in figure 5. The inviscid two-dimensional pressure differences and isobars as predicted by the method of characteristics solutions are also shown in these figures. The measured pressure differences in figure 4 generally agree with the inviscid theory which does not account for boundary-layer crossflow effects even though crossflow is known to occur along the sidewalls. The pressure differential measured on the center line of the top and bottom plates is generally less than the pressure differential measured on the top and bottom of the sidewalls.

Sidewall pressure measurements similarly agreed with the static pressures predicted by inviscid theory as seen in figure 5. In figure 5 the theory and data are presented in isobar form with the mirror image of the asymmetric nozzle comparing the experimental data with the theoretical predictions. The contours drawn through the experimental data by using the theory as a guide were drawn as smooth curves because of the uncertainty of determining the pressure gradients between the pressure orifices.

The agreement between the inviscid predictions and the measured wall pressures indicate that even when crossflow occurs in the boundary layer, the inviscid pressure gradients driving the crossflow could be used in a crossflow theoretical model, at least for the conditions of this experiment. The discrepancy that does exist between the predicted and measured wall-pressure distributions results from no allowance for the boundary-layer growth on the flat walls in the design of the nozzles. A boundary-layer correction was applied to the contoured wall.

Impact-Pressure Surveys

Impact-pressure traverses were made in the y-direction at constant values of the z-coordinate at the exit plane of each nozzle. A large number of traverses were measured of which figures 6 and 7 are typical. The numerous points measured in the exit plane of each nozzle were then plotted as a function of y and z and isobars were contoured through the data as illustrated in figure 8. These impact pressure traverses and isobar contours suggest the effects of crossflow in the boundary layer by the existence of

total pressure losses along the sidewalls. In the traverse of figure 6, the two-dimensional turbulent boundary-layer analysis predicts the total-pressure distribution very well with the exception of the outer region of the boundary layer on the flat bottom plate. The traverse shown in figure 7 indicates the pressure loss due to crossflow very near the sidewall. The isobars of figure 8 show lines of constant values of impact pressure ratio for half of the exit region of each nozzle. The indication of secondary flow down the sidewall is clearly discernible.

For the asymmetric nozzles studied in this experiment, the crossflow effects appear to be generally contained in the boundary layer. An interpretation of the crossflow effects in the corner regions of the nozzle will not be attempted in this analysis. The contours of figure 8 also show that the crossflow effects at the exit are no more severe for the higher turning angle nozzle even though the driving force is larger. This condition is due to the compensating effect between increased crossflow driving force in the large turning angle nozzle as compared with the thicker boundary-layer buildup in the longer, but smaller turning angle nozzle. Since the crossflow effects are largely contained in the boundary layer, a reasonable undisturbed flow core was measured for the three test nozzles. A comparison of the flow core found in these asymmetric nozzles with the flow core in a full two-dimensional nozzle may be made by using the data of references 5 and 12. In the symmetrical two-dimensional nozzle, the test flow core is reduced by the distorted boundary-layer growth along the center line of the sidewalls due to boundary-layer crossflow from both contoured walls toward the sidewall center line.

Reynolds Number Effects

All the data shown up to figure 8 were taken at a Reynolds number of 4.64×10^5, based on the flow speed at the nozzle throat and the throat height. The experiment was then repeated for Reynolds numbers of 3.70×10^5 and 2.75×10^5 by reducing the nozzle stagnation pressure from 372 to 220 kN/m^2 and maintaining an exit pressure to allow full expansion in the nozzle. Figures 9 and 10 illustrate the typical effects of Reynolds number on the total-pressure traverse at the exit of the $23^{\circ}23'$ nozzle. The traverse at $z = 0.107$ mm from the sidewall in figure 9 for Reynolds numbers of 4.64×10^5 and 2.75×10^5 indicate a slightly greater total-pressure loss in the bottom plate region for the lower Reynolds number. The traverse at $z = 0.5$ mm from the sidewall in figure 10 which is inside the sidewall boundary layer indicates an even greater total-pressure loss at the lower Reynolds number. The increase in pressure loss is expected since the wall boundary-layer thickness increases with a decreasing Reynolds number. The effect of crossflow on this pressure loss is difficult to assess. Over the limited range of Reynolds number covered in this experiment, the effects are very small and the rest of the impact data is similar to that shown in figures 9 and 10. The static wall-pressure data show no Reynolds number effects as expected.

SUMMARY OF RESULTS

The crossflow effects in three contoured, two-dimensional, asymmetric nozzles have been experimentally investigated and the results are compared with theoretical predictions of nozzle flow by using an inviscid method of characteristics solution and two-dimensional turbulent boundary-layer calculations. The results of this study show that

1. Crossflow takes place in the three test nozzles including a nozzle with a maximum turning angle of $15^{\circ}17'$. The existence of crossflow on the sidewalls was verified by oil-flow studies.

2. Crossflow effects are mainly confined to the boundary-layer region of the two-dimensional aysmmetric nozzles. The boundary-layer distortions are evaluated by comparing the measured impact pressure variations with the predicted two-dimensional turbulent boundary-layer profiles. For a nozzle design, where crossflow is undesirable, there is a trade-off between increased crossflow driving force in the larger turning angle nozzle and the thicker boundary-layer buildup in the longer, smaller turning angle nozzle.

3. Static wall pressure measurements agree well with the predictions of the inviscid two-dimensional theory even though crossflow occurs and is not accounted for in the calculations.

4. A relatively undisturbed flow core suitable for wind-tunnel test facilities and rectangular engine nozzle configurations was found for the three test nozzles.

Langley Research Center
National Aeronautics and Space Administration
Hampton, Va. 23665
May 30, 1975

REFERENCES

1. Anders, John B.; Sebacher, Daniel I.; and Boatright, William B.: Fluid Flow Analysis of Hot-Core Hypersonic-Wind-Tunnel Nozzle Concept. NASA TN D-6768, 1972.

2. Henry, John R.; and Anderson, Griffin Y.: Design Considerations for the Airframe-Integrated Scramjet. NASA TM X-2895, 1973.

3. Owczarek, J. A.; and Rockwell, D. O.: An Experimental Study of Flows in Planar Nozzles. Trans. ASME, Ser. D: J. Basic Eng., vol. 94, no. 3, Sept. 1972, pp. 682-688.

4. Pfenninger, W.; and Syberg, J.: Reduction of Acoustic Disturbances in the Test Section of Supersonic Wind Tunnels by Laminarizing Their Nozzle and Test Section Wall Boundary Layers by Means of Suction. NASA CR-2436, 1974.

5. Haefeli, Rudolph C.: Use of Fences To Increase Uniformity of Boundary Layer on Side Walls of Supersonic Wind Tunnels. NACA RM E52E19, 1952.

6. Ferri, Antonio: The Method of Characteristics. General Theory of High Speed Aerodynamics, W. R. Sears, ed., Princeton Univ. Press, 1954, pp. 583-669.

7. Dash, S.: The Determination of Nozzle Contours for Rotational, Non-Homentropic Gas Mixtures. ATL TR 148, Advanced Technology Laboratories, Inc., Mar. 1970.

8. McBride, Bonnie J.; Heimel, Sheldon; Ehlers, Janet G.; and Gordon, Sanford: Thermodynamic Properties to 6000^{o} K for 210 Substances Involving the First 18 Elements. NASA SP-3001, 1963.

9. Ames Research Staff: Equations, Tables, and Charts for Compressible Flow. NACA Rep. 1135, 1953. (Supersedes NACA TN 1428.)

10. Anderson, E. C.; and Lewis, C. H.: Laminar or Turbulent Boundary-Layer Flows of Perfect Gases or Reacting Gas Mixtures in Chemical Equilibrium. NASA CR-1893, 1971.

11. Miner, E. W.; Anderson, E. C.; and Lewis, Clark H.: A Computer Program for Two-Dimensional and Axisymmetric Nonreacting Perfect Gas and Equilibrium Chemically Reacting Laminar, Transitional and/or Turbulent Boundary Layer Flows. Va. Polytechnic Institute Report. VPI-E-71-8, May 1971. (Available as NASA CR 132601.)

12. McLellan, Charles H.; Williams, Thomas W.; and Beckwith, Ivan E.: Investigation of the Flow Through a Single-Stage Two-Dimensional Nozzle in the Langley 11-Inch Hypersonic Tunnel. NACA TN 2223, 1950.

13. Jackson, Mary W.; Czarnecki, K. R.; and Monta, William J.: Turbulent Skin Friction at High Reynolds Numbers and Low Supersonic Velocities. NASA TN D-2687, 1965.

TABLE I.- SIDEWALL PRESSURE ORIFICE COORDINATES

x, cm	y, cm	x, cm	y, cm	x, cm	y, cm
θ_{max} = 15°17' nozzle		θ_{max} = 23°23' nozzle		θ_{max} = 29°20' nozzle	
0.00	0.00	0.00	0.00	0.38	0.00
.00	.72	.00	.63	.38	.88
1.78	.45	1.73	.00	1.30	.00
3.38	.00	1.73	.84	1.30	1.30
3.38	.82	3.36	.00	2.60	.00
5.35	.70	3.36	1.38	2.60	.92
7.29	.06	5.02	.00	2.60	1.96
7.29	1.32	5.02	1.20	3.85	.00
9.00	.70	5.02	2.08	3.85	.93
10.70	.10	6.78	.06	3.85	2.55
10.70	2.00	6.78	1.20	5.10	.00
12.23	1.45	6.78	2.20	5.10	1.67
14.10	.10	8.55	1.20	5.10	2.98
14.10	1.45	10.10	.09	6.80	.04
14.10	2.90	10.10	1.73	6.80	1.67
15.78	2.00	10.10	3.60	6.80	3.45
17.50	.15	11.90	1.73	8.52	1.67
17.50	2.00	13.48	.10	10.18	.13
17.50	3.60	13.48	2.45	10.18	2.45
20.88	2.50	13.48	4.23	10.18	4.30
24.28	.23	15.15	2.45	11.95	2.45
24.28	2.50	16.88	.12	13.54	.20
24.28	4.40	16.88	2.45	13.54	2.45
27.28	2.50	16.88	4.25	13.54	4.89
31.08	.30	22.00	2.45	15.30	2.45
31.08	2.50	23.63	.12	17.16	.20
31.08	5.30	23.63	2.45	17.16	2.45
37.80	.40	23.63	5.40	17.16	5.25
37.80	2.50	26.60	2.45	20.51	2.45
37.80	5.62	30.45	.24	24.03	.30
		30.45	2.45	24.03	2.45
		30.45	5.62	24.03	5.50

TABLE II.- AXIAL DISTANCES FOR PRESSURE ORIFICES ALONG CENTER LINE OF CONTOURED PLATE AND FLAT BOTTOM PLATE

x, cm	x, cm	x, cm
θ_{max} = 15°17' nozzle	θ_{max} = 23°23' nozzle	θ_{max} = 29°20' nozzle
3.38	1.73	0.38
7.29	3.36	1.30
10.70	5.02	2.60
14.10	6.78	3.85
17.50	10.10	5.10
24.28	13.48	6.80
31.08	16.88	10.18
37.80	23.63	13.54
	30.45	17.16
		24.03

TABLE III.- NOZZLE COORDINATES

(a) Approach

x, cm	y, cm
All nozzles	
-2.540	3.81000
-2.413	2.57810
-2.286	2.25806
-2.032	1.85166
-1.778	1.56210
-1.524	1.34874
-1.270	1.18364
-1.016	1.05410
-.762	.96520
-.508	.89916
-.254	.86614
.0	.85598

(b) Expansion

x, cm	y, cm	x, cm	y, cm	x, cm	y, cm
$\theta_{max} = 15^{o}17'$ nozzle		$\theta_{max} = 23^{o}23'$ nozzle		$\theta_{max} = 29^{o}20'$ nozzle	
0.2540	0.85598	0.2540	0.85598	0.2540	0.89916
.5080	.86360	.5080	.86614	.5080	1.02616
.7620	.86614	.7620	.88646	.7620	1.17094
1.0160	.87122	1.0160	.91694	1.0160	1.31572
1.2700	.87884	1.2700	.95250	1.2700	1.46050
1.5240	.88900	1.5240	.99822	1.5240	1.59512
1.7780	.90170	1.7780	1.05410	1.7780	1.73228
2.0320	.91440	2.0320	1.11506	2.0320	1.85928
2.2860	.92710	2.2860	1.18618	2.2860	1.99390
2.5400	.94234	2.5400	1.25984	2.5400	2.11582
3.0480	.97536	3.0480	1.44526	3.0480	2.34950
3.5560	1.01854	3.5560	1.65354	3.5560	2.57302
4.0640	1.06680	4.0640	1.86690	4.0640	2.78130
4.5720	1.12014	4.5720	2.07264	4.5720	2.98450
5.0800	1.17348	5.0800	2.27330	5.0800	3.16992
6.3500	1.34620	6.3500	2.72288	5.5880	3.33756
7.6200	1.57226	7.6200	3.13436	6.0960	3.50012
8.8900	1.84404	8.8900	3.49504	6.6040	3.65252
10.1600	2.15646	10.1600	3.82778	7.1120	3.79984
11.4300	2.48920	11.4300	4.13004	7.6200	3.93700
12.7000	2.82956	12.7000	4.39420	8.8900	4.26974
13.9700	3.15468	13.9700	4.63042	10.1600	4.53898
15.2400	3.46202	15.2400	4.84378	11.4300	4.78282
16.5100	3.73126	16.5100	5.03936	12.7000	5.00634
17.7800	3.98780	17.7800	5.20700	13.9700	5.19938
19.0500	4.23672	19.0500	5.36194	15.2400	5.36956
20.3200	4.45516	20.3200	5.49910	16.5100	5.51180
21.5900	4.65328	21.5900	5.61594	17.7800	5.63372
22.8600	4.83870	22.8600	5.72262	19.0500	5.75056
24.1300	5.01650	24.1300	5.81406	20.3200	5.84200
25.4000	5.18160	25.4000	5.90042	21.5900	5.91820
26.6700	5.32892	26.6700	5.96646	22.8600	5.97662
27.9400	5.45846	27.9400	6.02234	24.1300	6.02996
29.2100	5.57530	29.2100	6.06298	25.4000	6.05790
30.4800	5.67436	30.4800	6.09092	26.6192	6.07314
31.7500	5.77088	31.2928	6.09854		
33.0200	5.86486				
34.2900	5.93852				
35.5600	6.00202				
36.8300	6.05790				
38.1000	6.10108				
39.3700	6.13410				
40.6400	6.16204				
42.1132	6.18490				

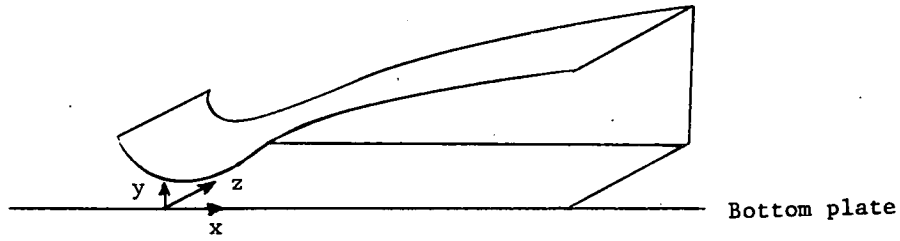

(a) Nozzle coordinates.

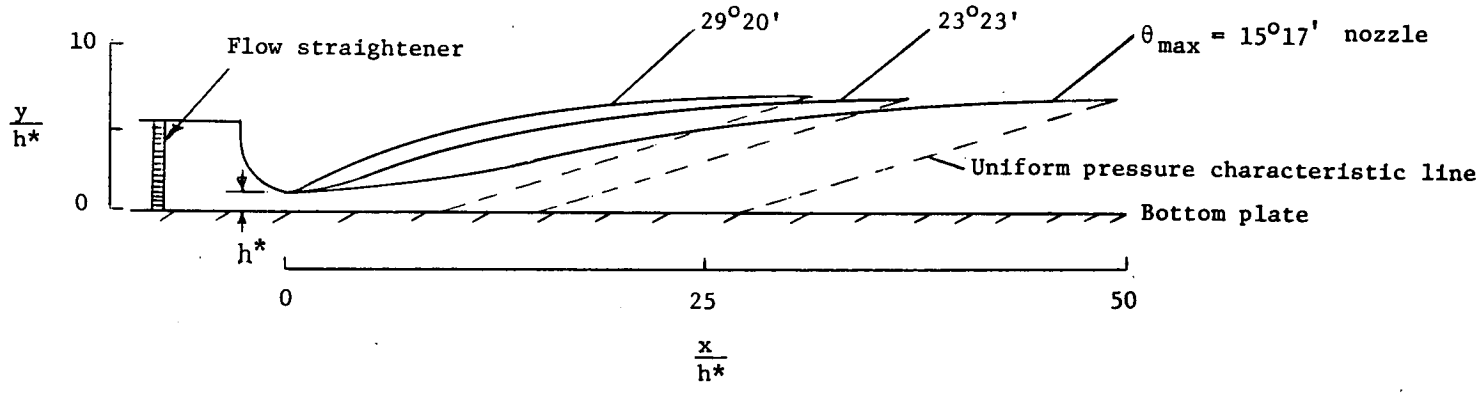

(b) Side view of three asymmetric nozzles investigated.

Figure 1.- Asymmetric nozzles.

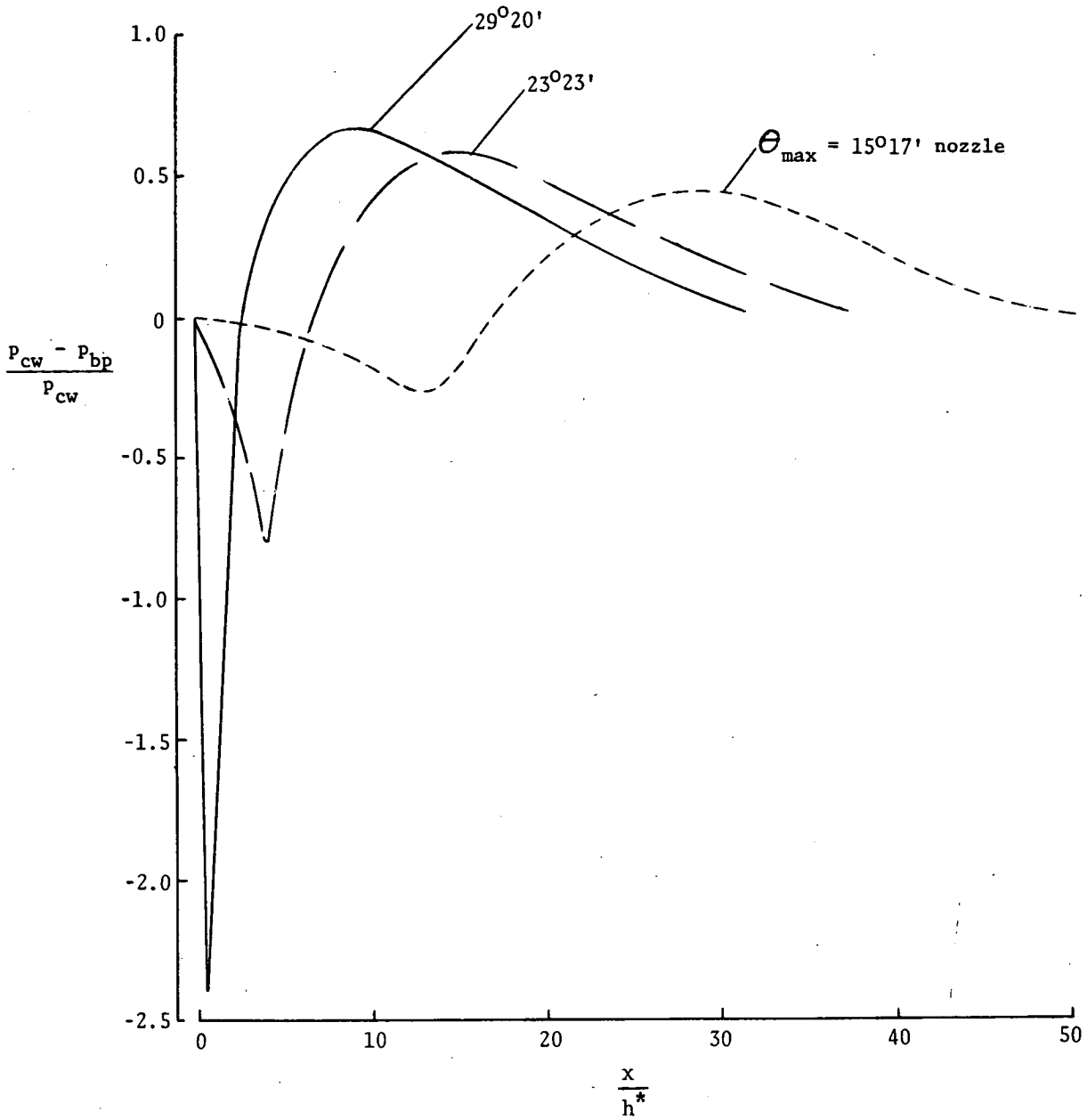

Figure 2.- Predicted pressure differences between top contoured plate and asymmetric nozzle bottom plate plotted against axial distance by using 2-D inviscid method of characteristic solutions.

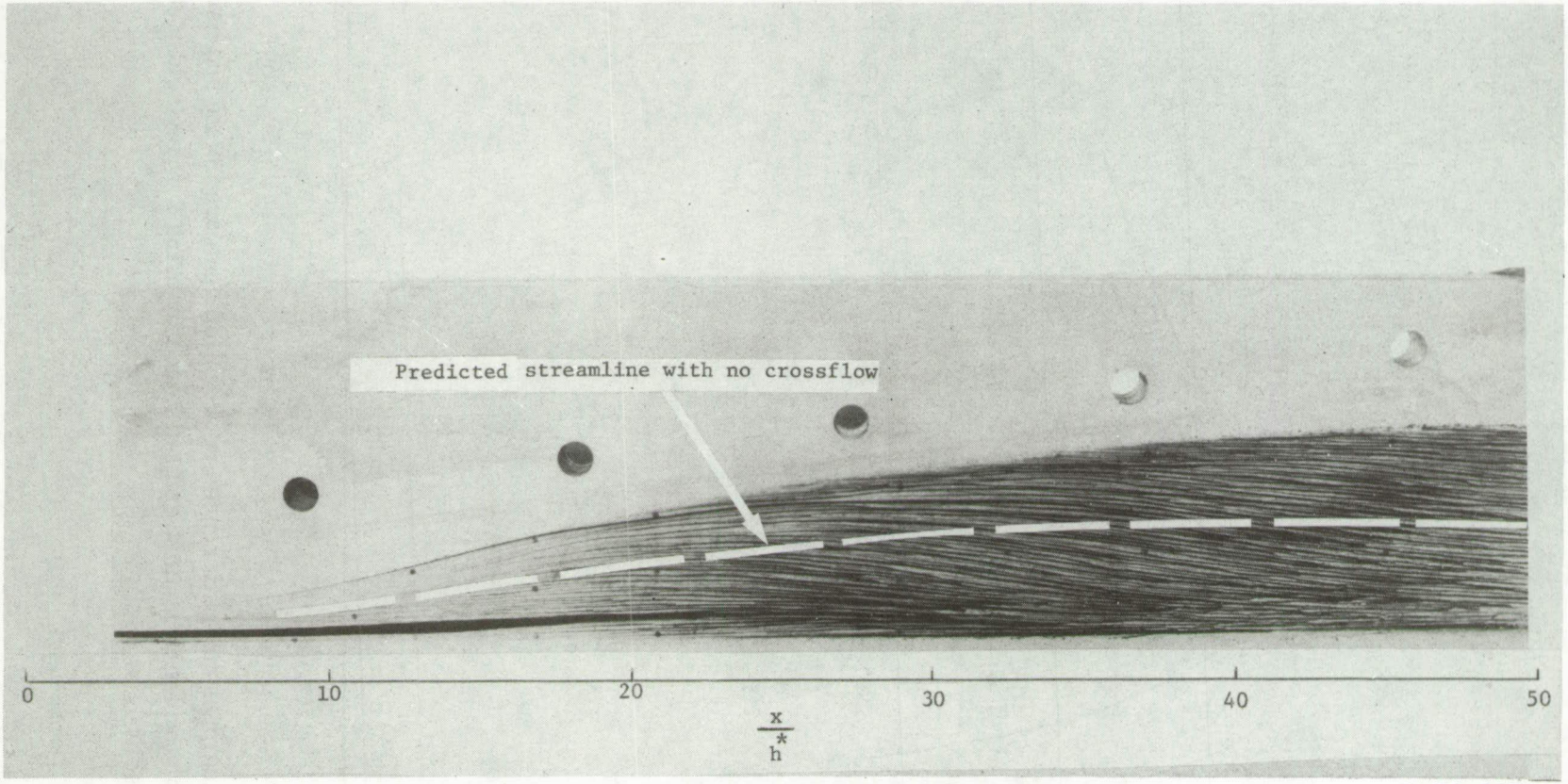

L-74-6076.1

(a) Side plate of $\theta_{max} = 15^{o}17'$ nozzle.

Figure 3.- Oil-flow visualization showing crossflow effects.

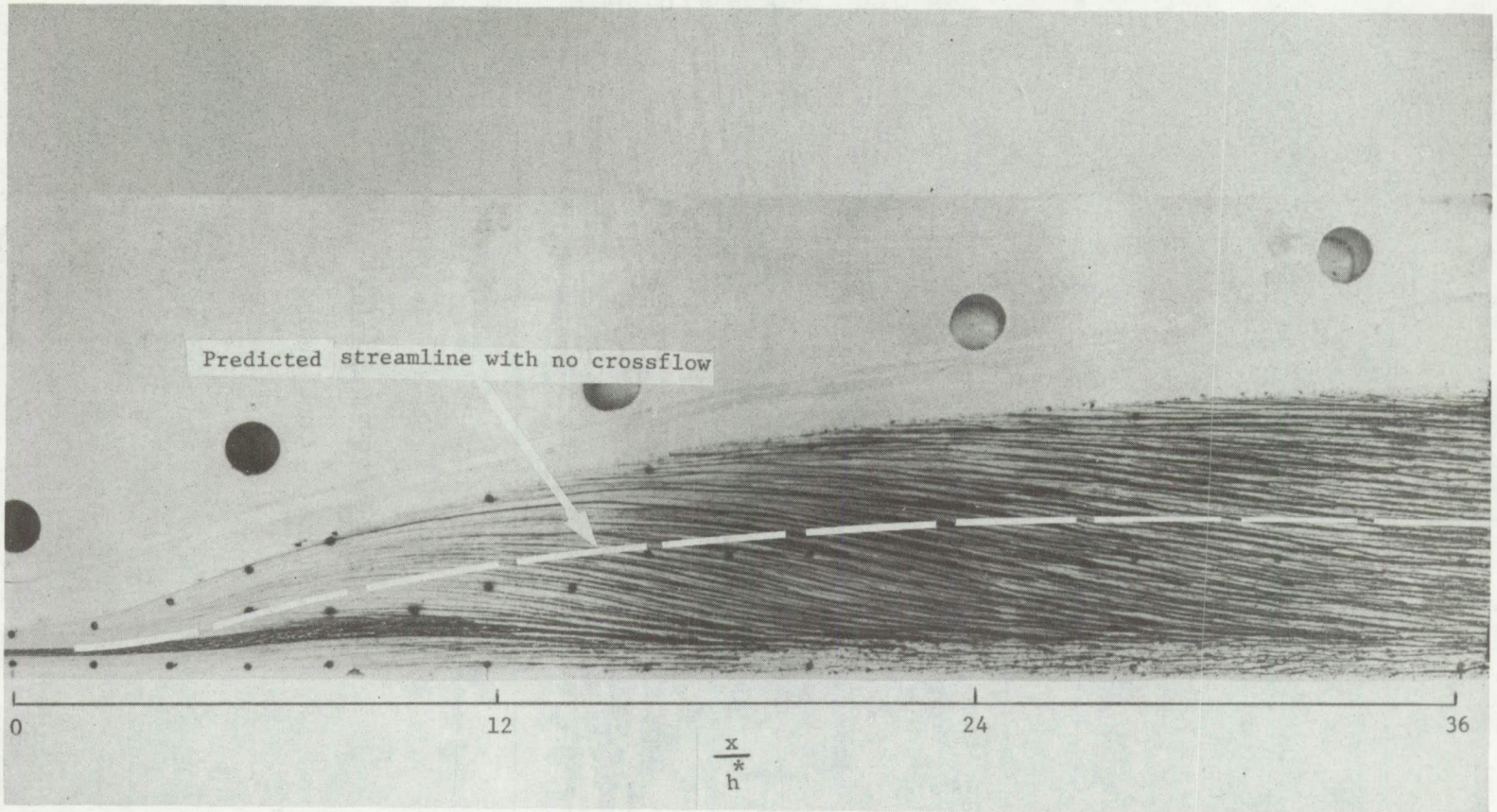

L-74-6215.1

(b) $\theta_{max} = 23^{o}23'$ nozzle.

Figure 3.- Continued.

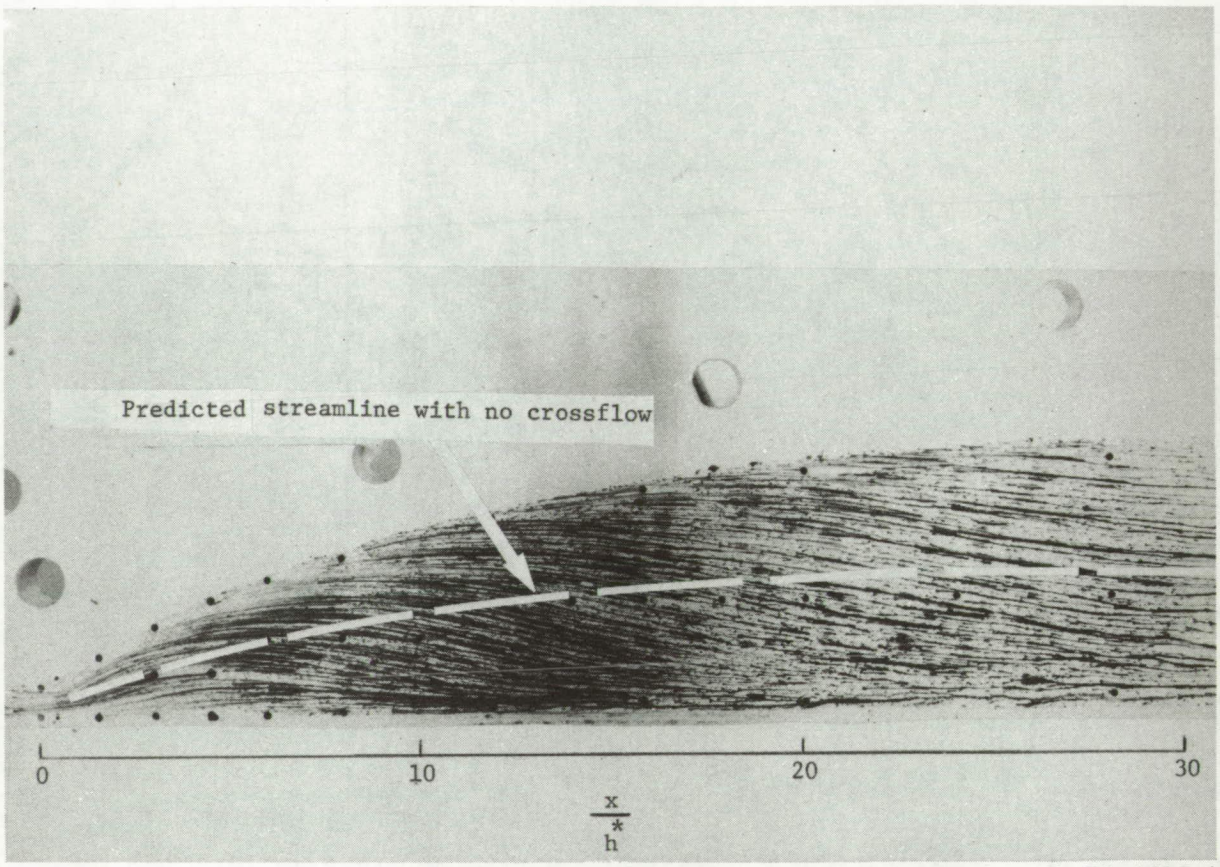

L-74-4473.1

(c) $\theta_{max} = 29^{o}29'$ nozzle.

Figure 3.- Concluded.

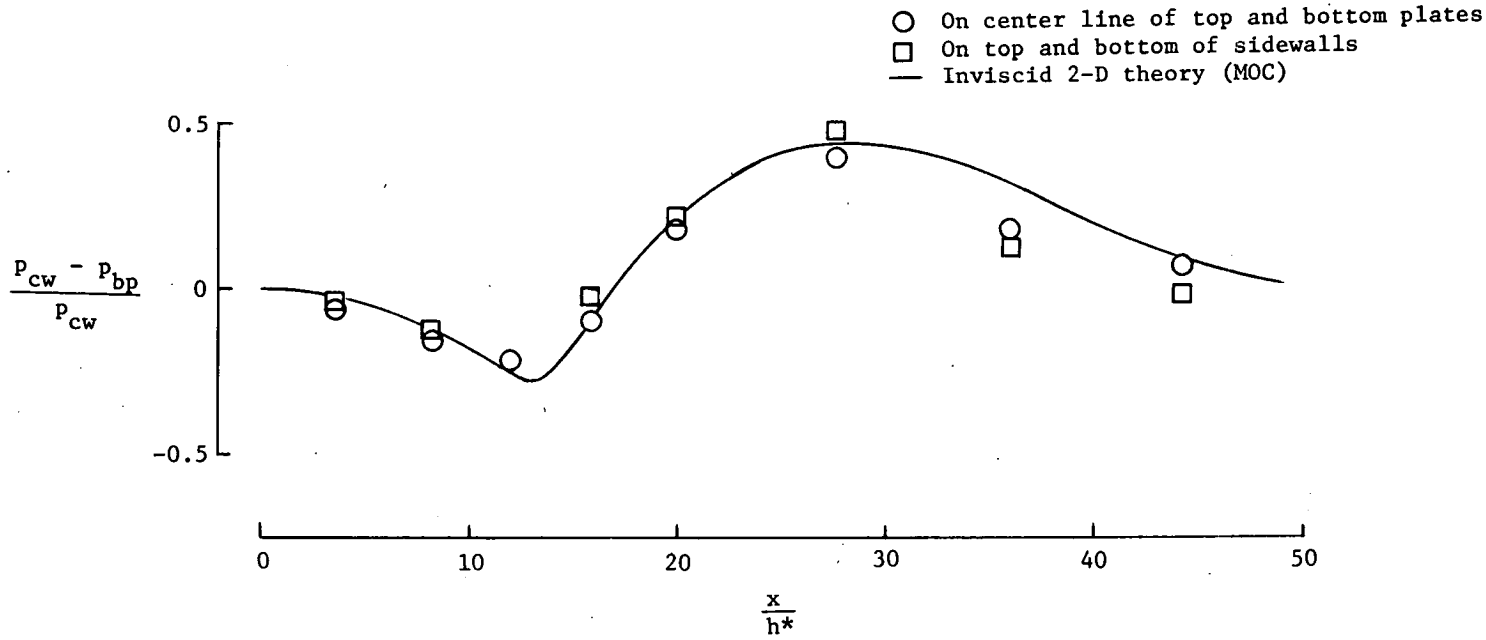

(a) $\theta_{max} = 15^{o}17'$.

Figure 4.- Measured and predicted pressure difference between top contoured plate and asymmetric nozzle bottom plate as a function of nozzle length.

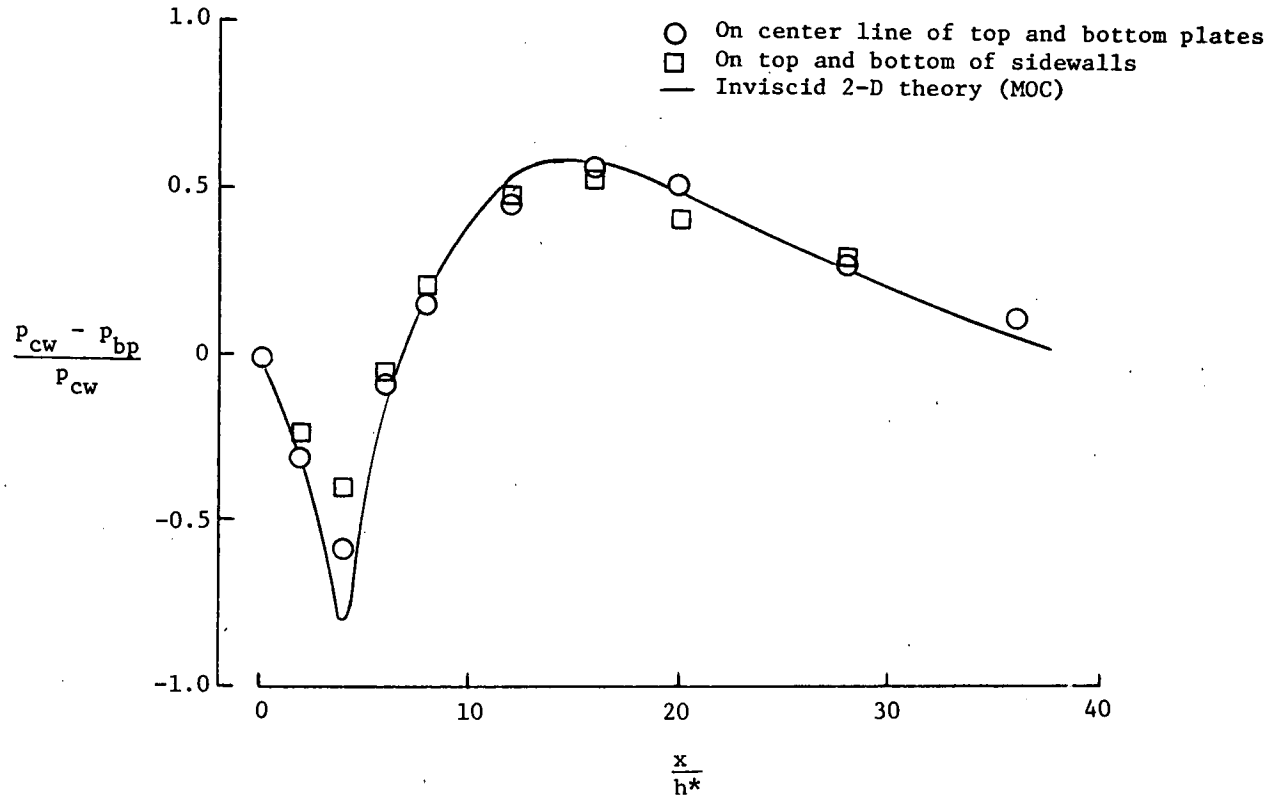

(b) $\theta_{max} = 23^{o}23'$ nozzle.

Figure 4.- Continued.

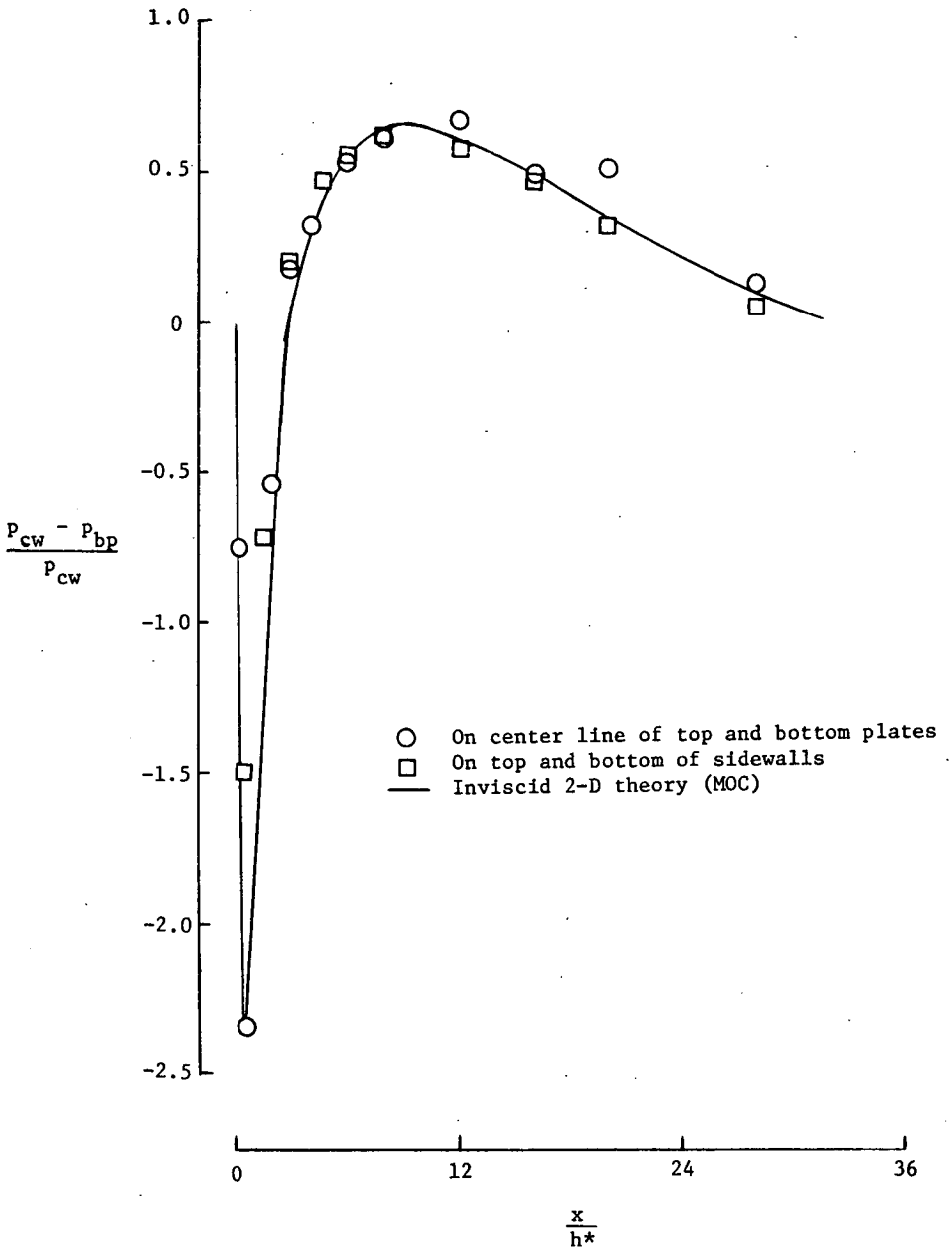

(c) $\theta_{max} = 29^{o}20'$ nozzle.

Figure 4.- Concluded.

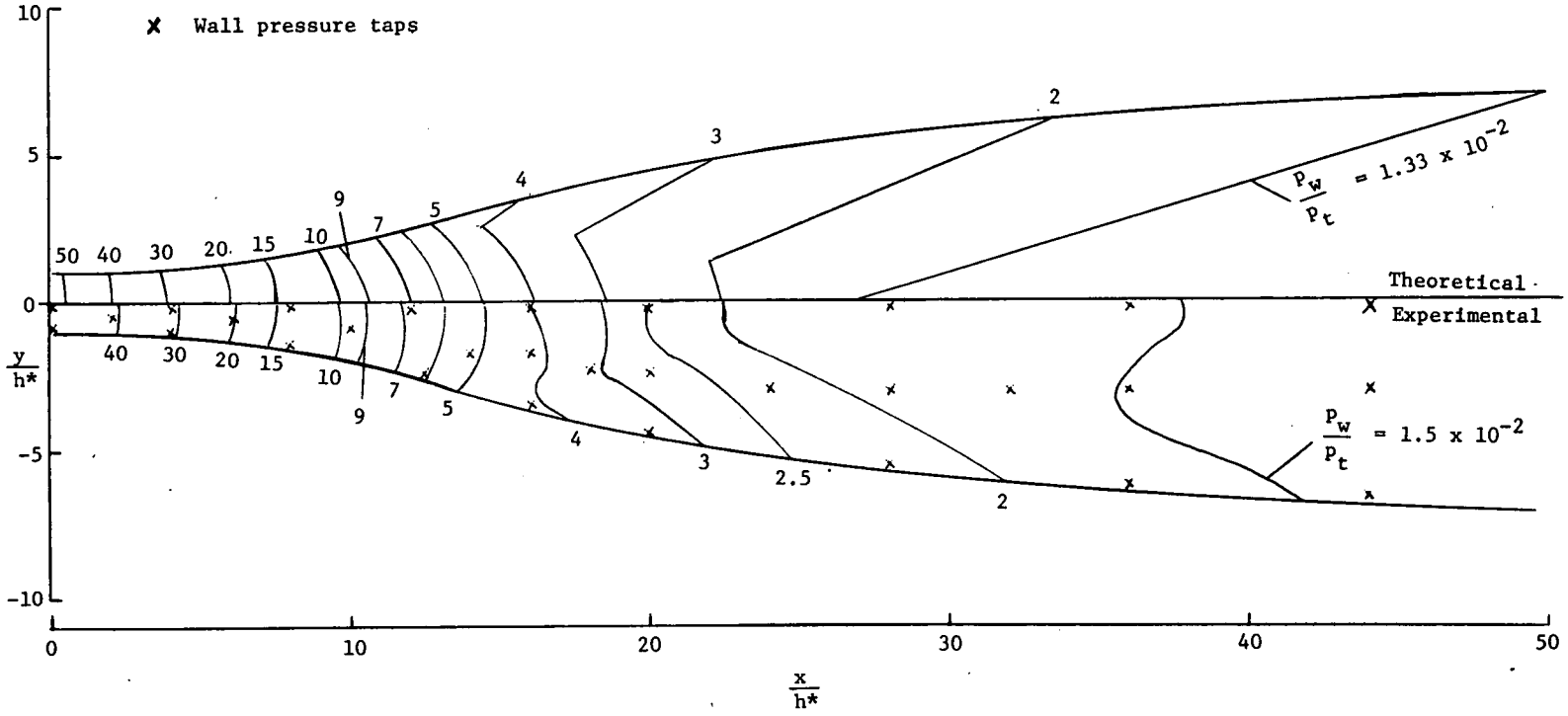

(a) $\theta_{max} = 15^{o}17'$ nozzle.

Figure 5.- Measured and predicted pressure contours on side plates.

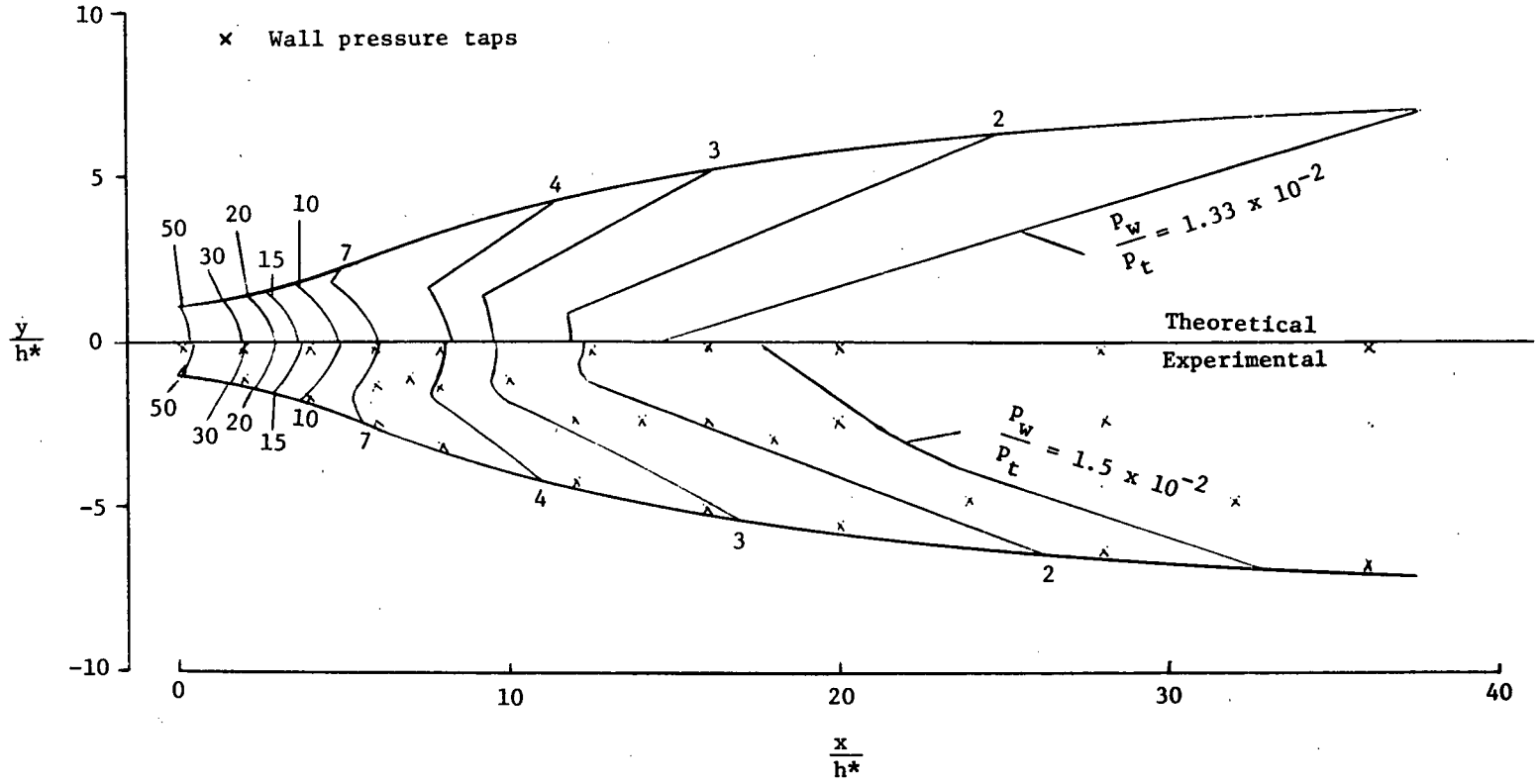

(b) $\theta_{max} = 23^{o}23'$ nozzle.

Figure 5.- Continued.

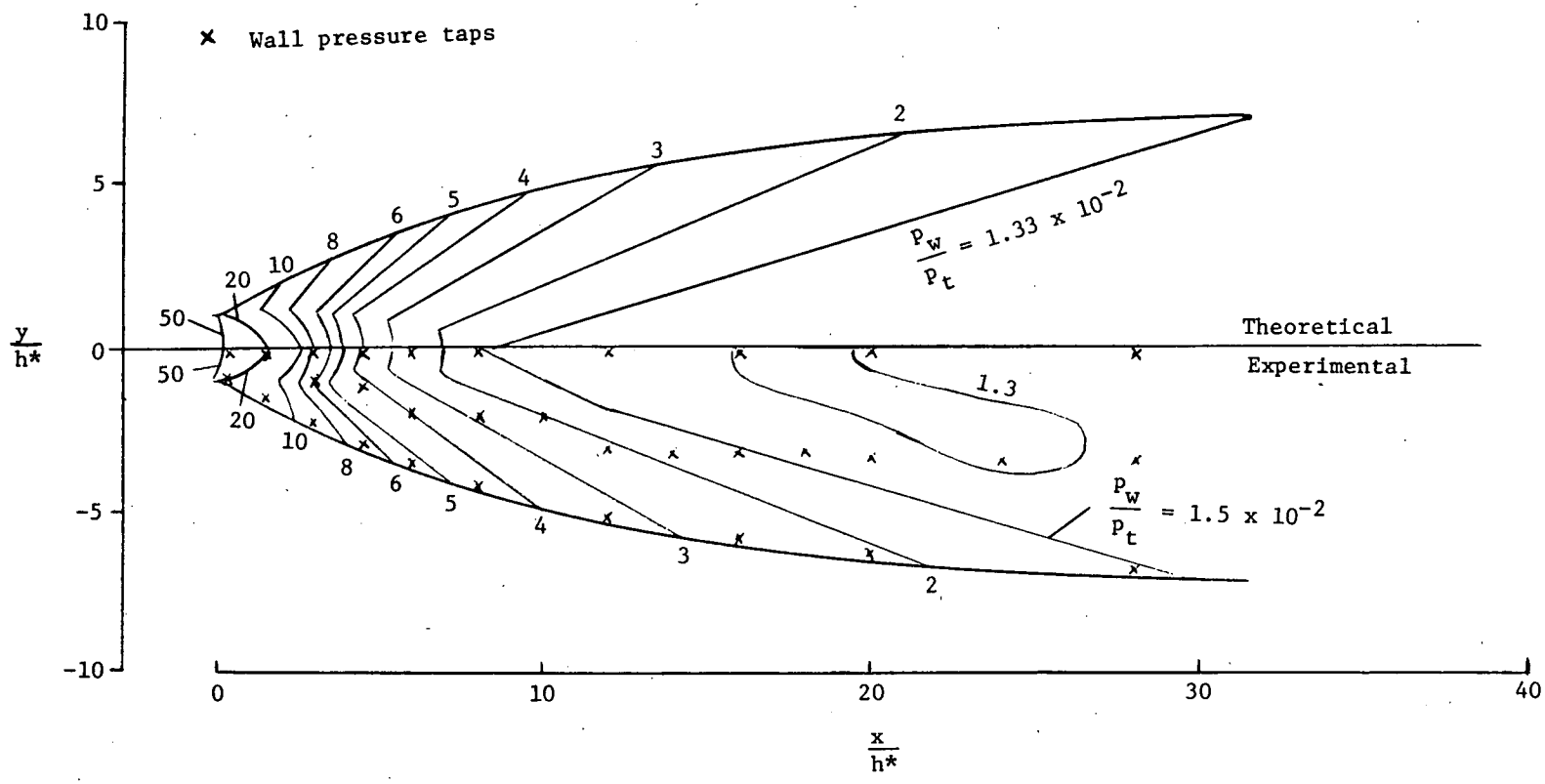

(c) $\theta_{max} = 29^{o}20'$ nozzle.

Figure 5.- Concluded.

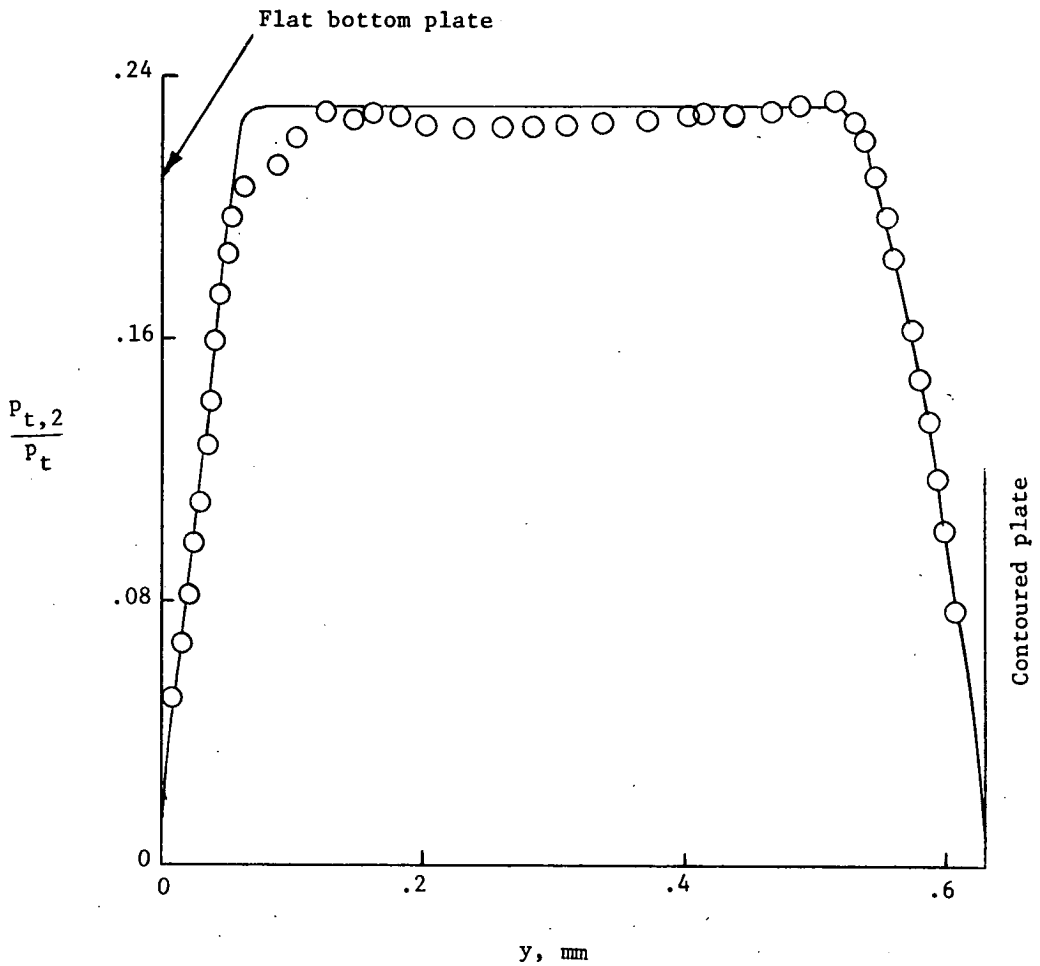

Figure 6.- Typical measured and predicted impact pressure ratio profiles at exit plane against vertical station at $z = 0.107$ mm from side plate. $\theta_{max} = 23^{o}23'$; $N_{Re} = 4.64 \times 10^{5}$.

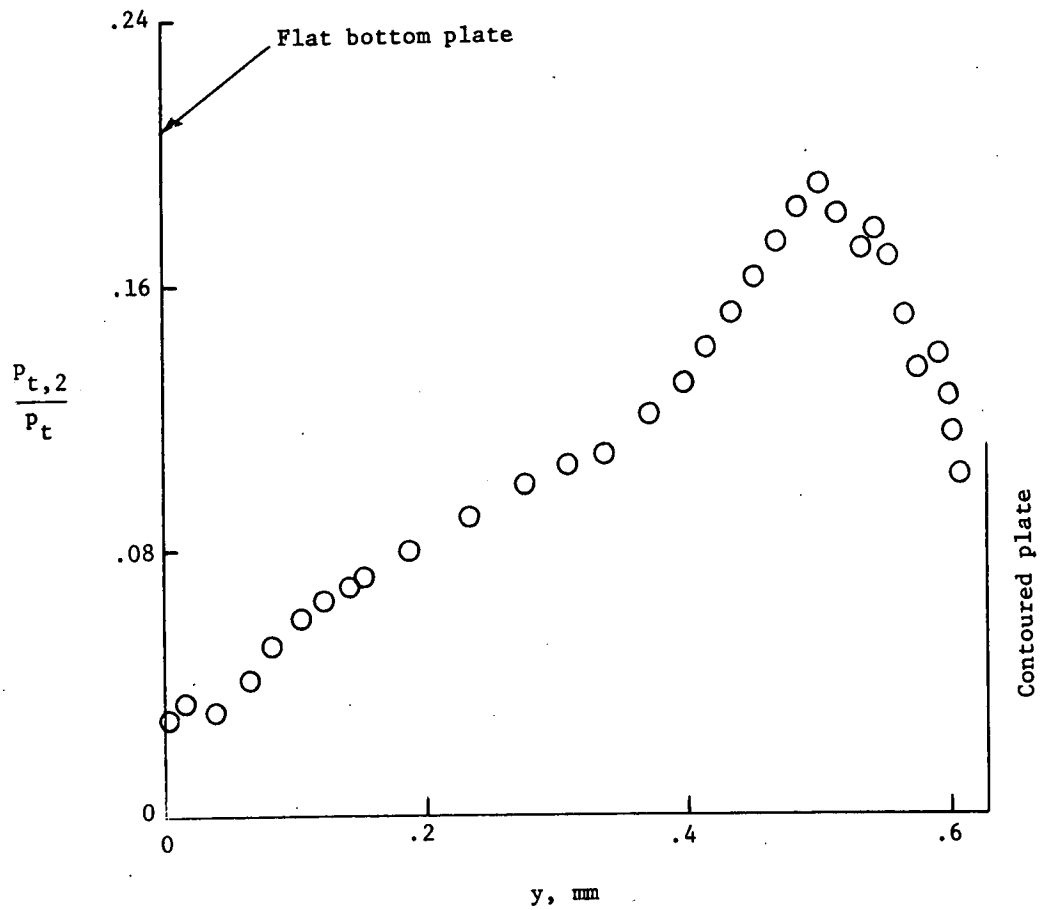

Figure 7.- Typical measured impact pressure ratio profiles at exit plane plotted against vertical station at $z = 0.5$ mm from side plate. $\theta_{max} = 23^{o}23'$; $N_{Re} = 4.64 \times 10^{5}$.

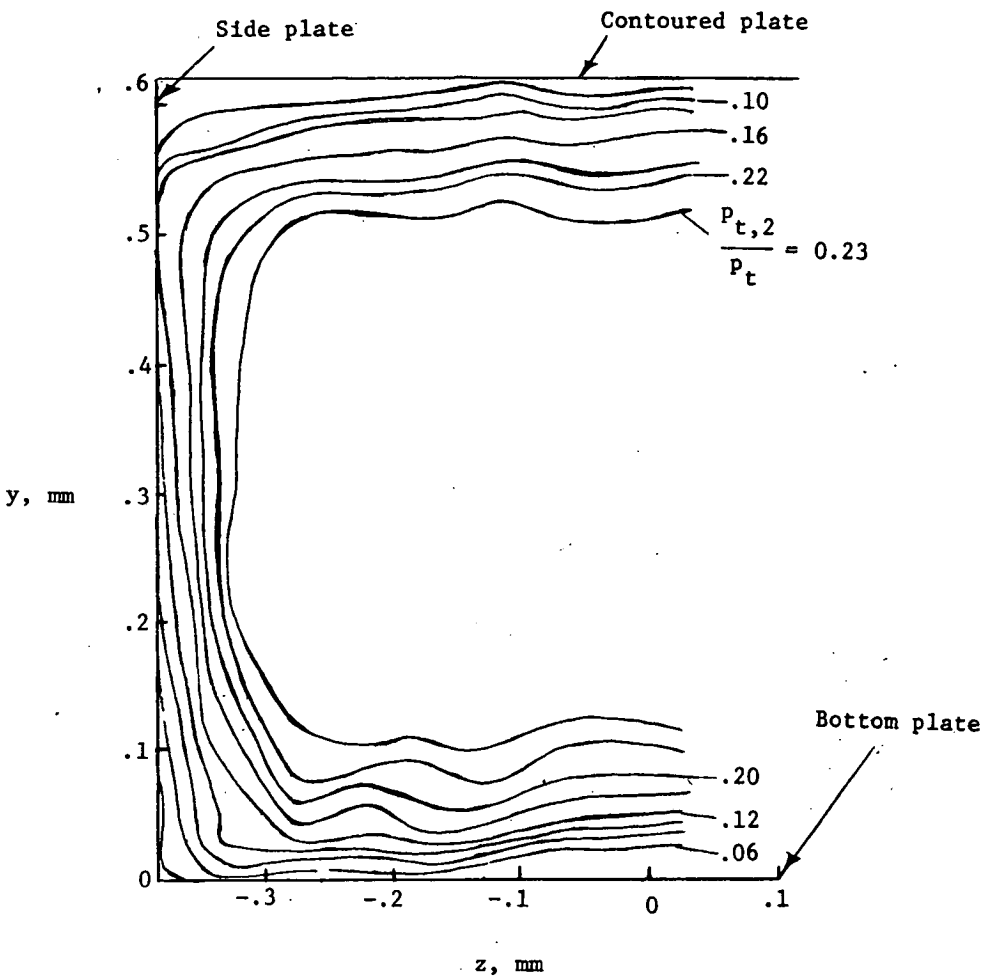

(a) $\theta_{max} = 15^{o}17'$; $N_{Re} = 4.64 \times 10^{5}$.

Figure 8.- Measured impact pressure ratio contours at exit of nozzle constructed from plots similiar to figures 4 and 5.

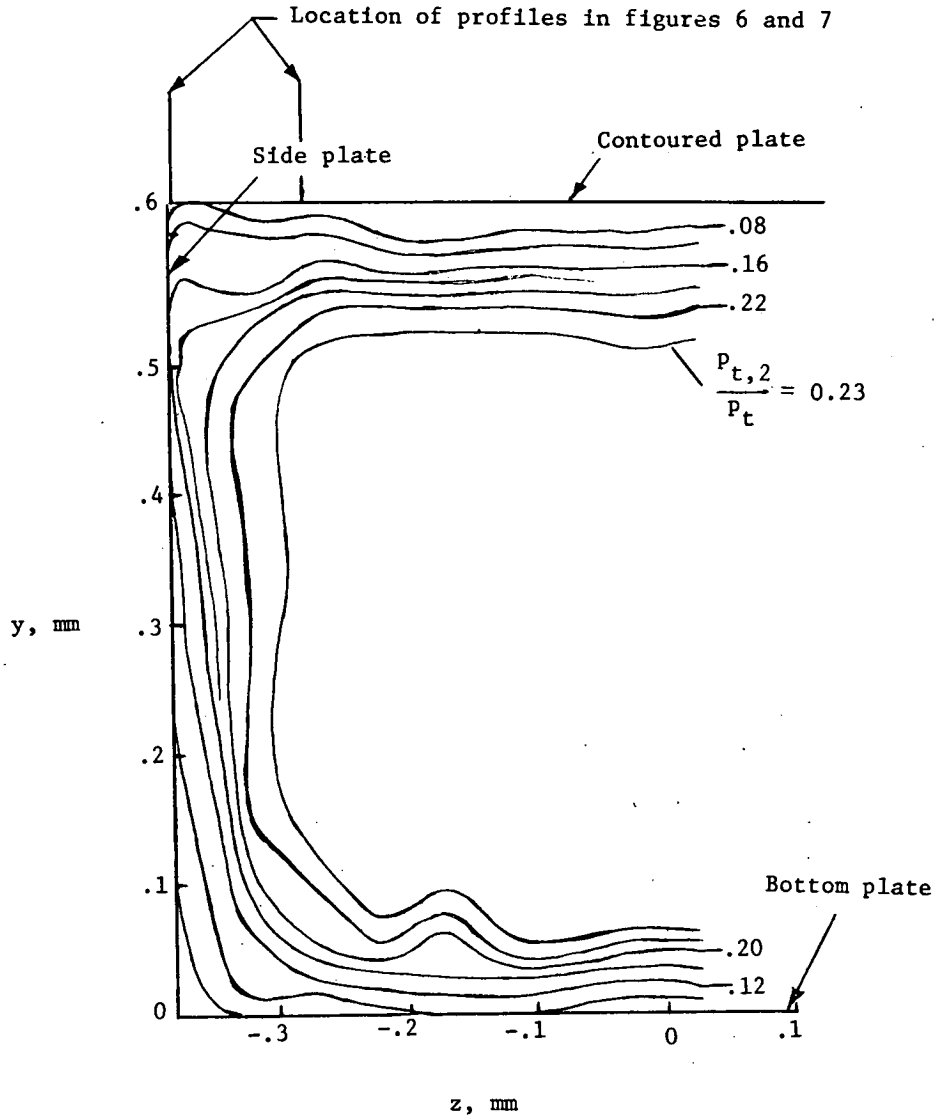

(b) $\theta_{max} = 23^{o}23'$ nozzle; $N_{Re} = 4.64 \times 10^5$.

Figure 8.- Continued.

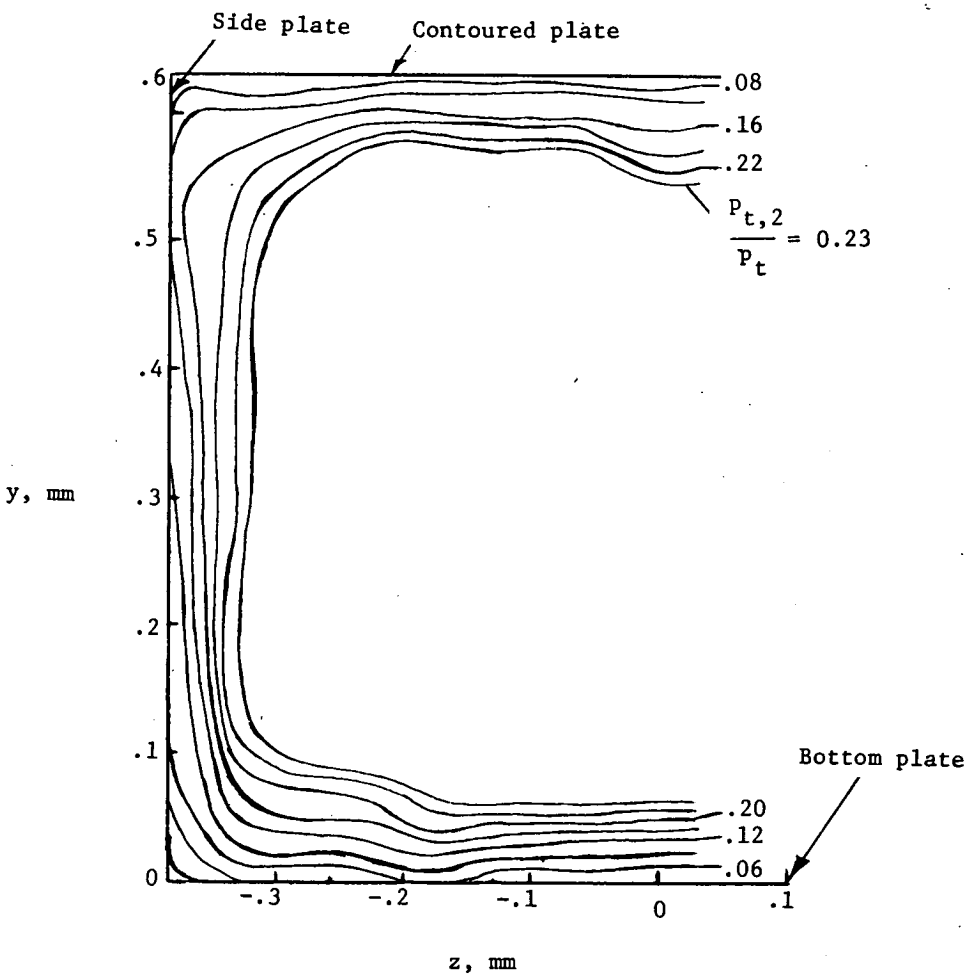

(c) $\theta_{max} = 29^{o}20'$ nozzle; $N_{Re} = 4.64 \times 10^5$.

Figure 8.- Concluded.

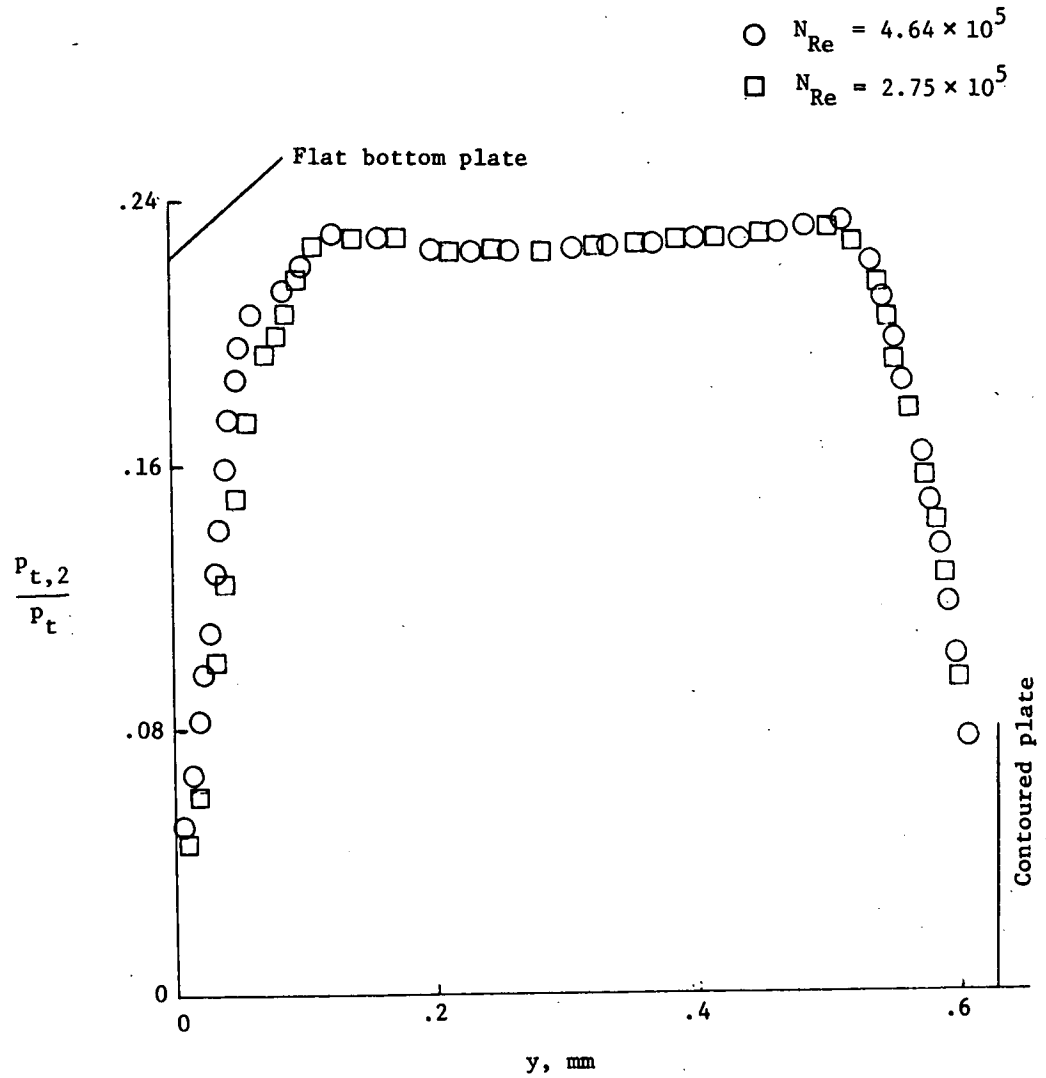

Figure 9.- Typical measured impact pressure ratio profiles at exit plane plotted against vertical station at $z = 0.107$ mm from side plate. $\theta_{max} = 23^{\circ}23'$.

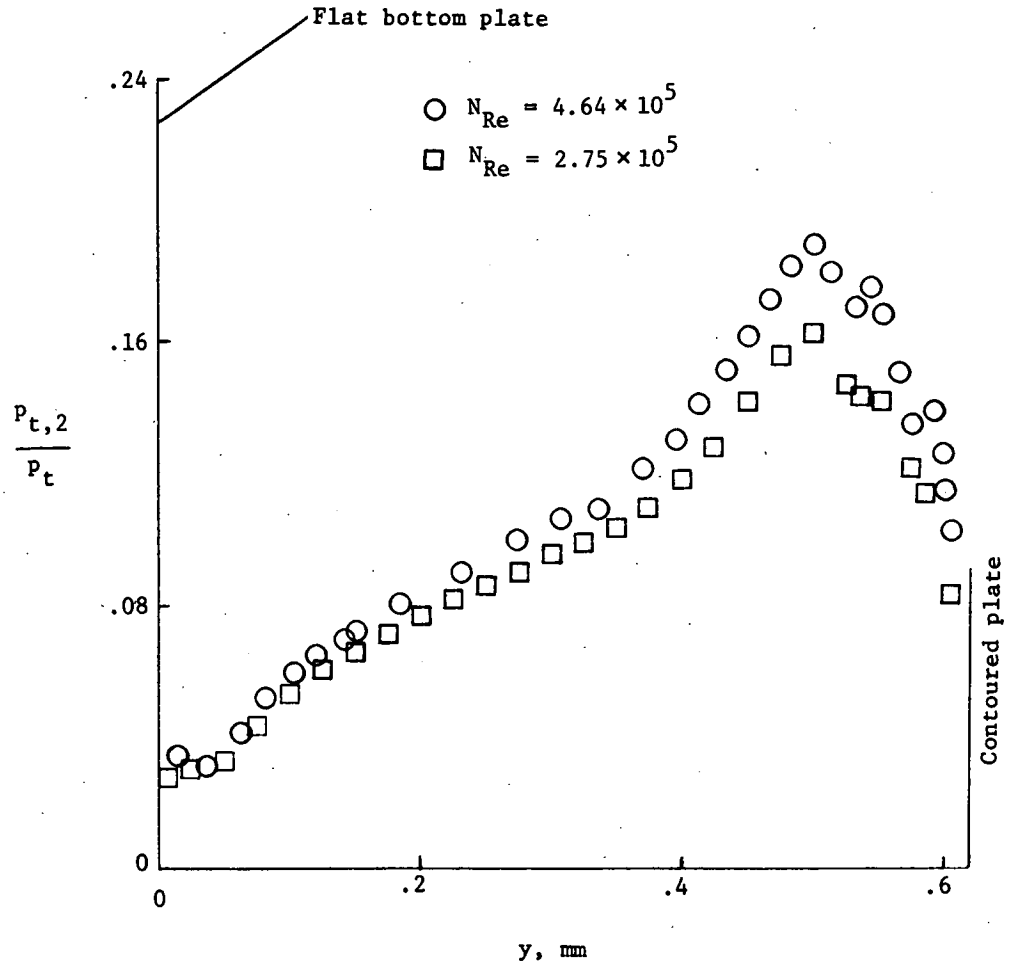

Figure 10.- Typical measured impact pressure ratio profiles at exit plane plotted against vertical station at $z = 0.5$ mm from side plate. $\theta_{max} = 23^{o}23'$.

NATIONAL AERONAUTICS AND SPACE ADMINISTRATION
WASHINGTON, D.C. 20546

OFFICIAL BUSINESS
PENALTY FOR PRIVATE USE $300

SPECIAL FOURTH-CLASS RATE BOOK

POSTAGE AND FEES PAID
NATIONAL AERONAUTICS AND SPACE ADMINISTRATION
451

U.S.MAIL

POSTMASTER: If Undeliverable (Section 158 Postal Manual) Do Not Return

"The aeronautical and space activities of the United States shall be conducted so as to contribute . . . to the expansion of human knowledge of phenomena in the atmosphere and space. The Administration shall provide for the widest practicable and appropriate dissemination of information concerning its activities and the results thereof."

—NATIONAL AERONAUTICS AND SPACE ACT OF 1958

NASA SCIENTIFIC AND TECHNICAL PUBLICATIONS

TECHNICAL REPORTS: Scientific and technical information considered important, complete, and a lasting contribution to existing knowledge.

TECHNICAL NOTES: Information less broad in scope but nevertheless of importance as a contribution to existing knowledge.

TECHNICAL MEMORANDUMS: Information receiving limited distribution because of preliminary data, security classification, or other reasons. Also includes conference proceedings with either limited or unlimited distribution.

CONTRACTOR REPORTS: Scientific and technical information generated under a NASA contract or grant and considered an important contribution to existing knowledge.

TECHNICAL TRANSLATIONS: Information published in a foreign language considered to merit NASA distribution in English.

SPECIAL PUBLICATIONS: Information derived from or of value to NASA activities. Publications include final reports of major projects, monographs, data compilations, handbooks, sourcebooks, and special bibliographies.

TECHNOLOGY UTILIZATION PUBLICATIONS: Information on technology used by NASA that may be of particular interest in commercial and other non-aerospace applications. Publications include Tech Briefs, Technology Utilization Reports and Technology Surveys.

Details on the availability of these publications may be obtained from:

SCIENTIFIC AND TECHNICAL INFORMATION OFFICE

NATIONAL AERONAUTICS AND SPACE ADMINISTRATION

Washington, D.C. 20546